# Exosomal miR-142-3p secreted by hepatitis B virus (HBV)-hepatocellular carcinoma (HCC) cells promotes ferroptosis of M1-type macrophages through SLC3A2 and the mechanism of HCC progression

**Zongqiang Hu[1#], Yanfeng Yin[2#], Jie Jiang[1#], Chuntao Yan[2], Yiting Wang[2], Dongdong Wang[1], Li Li[1]**

[1]Hepato-Pancreato-Biliary Surgery Department, The First People's Hospital of Kunming & The Calmette Affiliated Hospital of Kunming Medical University, Kunming, China; [2]The Central Laboratory, The First People's Hospital of Kunming & The Calmette Affiliated Hospital of Kunming Medical University, Kunming, China

*Contributions:* (I) Conception and design: Z Hu, L Li; (II) Administrative support: Y Yin, J Jiang, L Li; (III) Provision of study materials or patients: C Yan, Y Wang; (IV) Collection and assembly of data: Z Hu, Y Yin, J Jiang; (V) Data analysis and interpretation: Z Hu, Y Yin, J Jiang; (VI) Manuscript writing: All authors; (VII) Final approval of manuscript: All authors.

[#]These authors contributed equally to this work and should be considered as co-first authors.

*Correspondence to:* Li Li. Hepato-Pancreato-Biliary Surgery Department, The First People's Hospital of Kunming & The Calmette Affiliated Hospital of Kunming Medical University, No. 1228 Beijing Road, Kunming 650032, China. Email: ynkmlili62@hotmail.com.

**Background:** Most patients with hepatitis B virus (HBV) infection will develop hepatocellular carcinoma (HCC). This study aimed to explore the potential mechanism of miR-142-3p in HCC caused by HBV infection.

**Methods:** HepG2 cells and M1 macrophages were cocultured and then infected with HBV to establish an *in vitro* model. MicroRNA (miRNA) and messenger RNA (mRNA) expression was analyzed by quantitative reverse transcription polymerase chain reaction (RT-qPCR) and Western blot. The protein expressions of COX2, ACSL4, PTGS2, GPX4, and NOX1 were analyzed by Western blot. Flow cytometry and TUNEL assays were used to assess cell reactive oxygen species (ROS) and ferroptosis, respectively. Cell invasion and migration were measured by Transwell assay. To evaluate the ferroptosis of M1-type macrophages, glutathione (GSH), malondialdehyde (MDA), and $Fe^{2+}$ content was detected by corresponding kits. Dual luciferase reporter gene detection verified the targeting relationship between miR-142-3p and SLC3A2.

**Results:** MiR-142-3p was highly expressed in HBV-infected HCC patients and HBV-infected M1-type macrophages. Inhibition of miR-142-3p or overexpression of SLC3A2 reversed ferroptosis and inhibited the proliferation, migration, and invasion of HCC cells.

**Conclusions:** Our findings indicated that miR-142-3p promoted HBV-infected M1-type macrophage ferroptosis through SLC3A2, affecting the production of GSH, MDA, and $Fe^{2+}$ and accelerating the development of HCC. The regulation of miR-142-3p and its target genes will help to clarify the pathogenesis of HCC induced by HBV infection and provide new theoretical foundations and therapeutic targets.

**Keywords:** MiR-142-3p; hepatitis B virus (HBV); hepatocellular carcinoma (HCC); SLC3A2

## Introduction

Hepatitis B virus (HBV) is the most common cause of chronic liver infection worldwide. Most patients with HBV infection will develop hepatocellular carcinoma (HCC) (1). Previous studies have suggested that compared with non-HBV carriers, chronic HBV infection may increase the risk of HCC by 200 times (2). HBV infection causes liver injury, including cirrhosis inflammation and fibrosis, which can promote oncogenic transformation (3). HBV is not cytopathic for hepatocytes, a characteristic that may lead to the delayed response of the immune system after HBV infection (4). As a major component of the tumor microenvironment (TME), tumor-associated macrophages (TAMs) play a critical role in the immune system (5). There are 2 types of macrophages in tissues: M1-type TAM can inhibit tumor growth and enhance immunity (6), and M2-type TAM plays a role in promoting and supporting the development of tumors. TAMs can inhibit the proliferation and activation of T cells, regulate and promote Th2 immune response, promote tumor cell growth, participate in tumor angiogenesis, and promote tumor infiltration and metastasis (7). The study found a strong association between increased macrophage density and poor survival in HCC (8). However, the role of TAMs in HBV-HCC remains unknown.

Exosomes are lipid bilayer vesicles with a diameter of 40–200 nm which are produced by most types of cells and released into body fluids such as urine, saliva, and blood (9). They play an important role in signal transduction between cells. Exosomes carry microRNA (miRNA) that control the expression of multiple target genes at the posttranscriptional level (10). The mature forms of these miRNAs are about 22 nucleotides long and mainly target the 3' untranslated region (3'-UTR), resulting in a decrease in the expression level of the target proteins (11). There is growing evidence that many viruses utilize exosomes as another route of transmission, with the additional benefit of being at least partially shielded from immune responses (12). Recently, it has been shown that exosomal miR-15b is an important miRNA involved in HBV infection and HCC development (13). The downregulated expression of miR-501 might provide a new mechanism and therapeutic target for inhibiting HBV replication (14). Further, exosomal miR-192, as a major regulator, may be a potential treatment target for HBV-mediated hepatic fibrosis (15).

In this study, we found that M1 macrophages were low in HBV-HCC tissue, while exosomal miR-142-3p was highly expressed. Studies have shown that miR-142-3p can affect macrophage differentiation, for example, miR-142-3p can prevent macrophage differentiation during cancer-induced bone marrow formation (16). Meanwhile, studies have found that HBV infection is closely related to the occurrence of ferroptosis, for example, exosome miR-222 from HBV-infected hepatocytes promotes liver fibrosis by inhibiting transferrin receptor (TFRC) and TFRC-induced ferroptosis (17). It has been reported that miR-142-3p can inhibit HCC metastasis by regulating HMGB1 gene expression (18), and this study found another role of miR-142-3p in exosomes of HBV infection-positive hepatoma cells, namely miR-142-3p can regulate ferroptosis of M1 macrophages by targeting SLC3A2, and promote the proliferation, migration and invasion of hepatoma cells. This study conducted an in-depth investigation of this molecular mechanism with a view to providing new ideas for the treatment of HCC. We present the following article in accordance with the MDAR reporting checklist (available at https://jgo.amegroups.com/article/view/10.21037/jgo-21-916/rc).

## Methods

### Sample collection

Data were collected from HCC patients at the Calmette Hospital Affiliated to Kunming Medical University (Kunming, Yunnan, China). Inclusion criteria were as follows: patients with no surgical history or other therapy treatments, and patients with no other primary tumor. The exclusion criteria were as follows: patients suffering from other severe disease, including hepatitis A, hepatitis C, hepatitis E, or human immunodeficiency virus (HIV) co-infection, heart, autoimmune liver disease, drug-induced hepatitis, fatty liver disease, or long-term history of alcohol. Based on the results of hepatitis B surface antigen (HBsAg) examination by serology and immunohistochemistry, patients were classified as HBV positive (HBV+) or negative (HBV−). The patient's HCC tissue, adjacent tissue, and serum samples were collected and stored at –80 ℃ until later use. The study was conducted in accordance with the Declaration of Helsinki (as revised in 2013). The present study was approved by the Medical Ethics Committee of the First People's Hospital of Kunming (No. YLS2020-08) and all participants signed informed consent forms.

## Cell culture

HepG2 and human monocytic cell line THP-1 were purchased from the Institutes for Biological Sciences at the Chinese Academy of Sciences (Shanghai, China). HepG2 cells were maintained in high-glucose Dulbecco's modified Eagle's medium (DMEM) supplemented with 10% fetal bovine serum (FBS) (Thermo Fisher Scientific, Waltham, MA, USA) and then placed in a humidified incubator at 37 ℃ and 5% $CO_2$.

THP-1 cells were maintained in Roswell Park Memorial Institute medium (RPMI 1640, Invitrogen, Carlsbad, CA, USA) supplemented with 10% FBS, penicillin (100 U/mL), streptomycin (100 µM), and β-mercaptoethanol (50 µM, Sigma-Aldrich, St. Louis, MO, USA). THP-1 monocytes were differentiated into macrophages via 24-hour incubation with phorbol 12-myristate 13-acetate (150 ng/mL, Sigma-Aldrich) followed by 24-hour incubation in RPMI medium. The macrophages were polarized to M1 macrophages using 50 ng/mL interferon gamma (IFN-γ) (PeproTech, East Windsor, NJ, USA) and 1 µg/mL lipopolysaccharide (LPS) (Sigma-Aldrich) for 24 hours.

## HBV virus infection

The cells were seeded at a concentration of $1{\times}10^5$ cells/culture dish. Two days after inoculation, the cells were incubated at 4 ℃ for 2 hours and then at 37 ℃ in an atmosphere containing 5% $CO_2$ for 6 hours. HepG2 cells were infected with HBV[+] serum (HBV particles $1{\times}10^{10}$ copies/mL) and cocultured in DMEM for 48 hours. The HBV[+] serum was then removed and the cells were washed with phosphate buffered saline (PBS) 8 times.

## Isolation of exosomes

The procedure of HBV[+]-induced hepatocarcinoma-derived exosome isolation was performed at 4 ℃. In short, the supernatant collected from the cultured HCC cells was first filtered through a 0.2-µm filter to remove large debris. Dead cells and small-cell debris were removed by centrifuge at 10,000 rpm for 30 minutes. The supernatant was then centrifuged at 10,000 rpm for another 3 hours. The supernatant produced in this step was stored at 4 ℃ for future use as a control without exosomes (the average storage time was no more than 1 week), and the pellet was resuspended in 30–50 µL PBS and stored at –80 ℃ for later use. After exosome extraction, the expressions of exosome markers HSP70, CD63, TSG101 and CD81 were detected by Western blot to characterize exosome.

## Cell transfection

To construct the SLC3A2 overexpression vector, an empty vector (pcDNA3.1, Invitrogen) was used as a negative control (NC). MiR-142-3p inhibitor and NC mimic (GenePharma, Shanghai, China) were then synthesized. Transfection was performed using Lipofectamine 3000 (Invitrogen) according to the manufacturer's instructions.

## Immunohistochemistry

All slices were cut to a thickness of 2 µm. BOND primary antibody diluent and the BOND Polymer Refine Detection kit (Leica Biosystems, Wetzlar, Germany) were used to perform immunohistochemical (IHC) staining on intact slides from formalin-fixed paraffin-embedded (FFPE) blocks using the Leica BOND RX automated immunostainer. Tumor cells were morphologically identified by cell shape, size, and nuclear configuration. Under a microscope, CD80^{+} and CD163^{+} staining in tumor cells was divided into 3 groups: 0 (no membrane or cytoplasmic staining), 1+ (weak or incomplete membrane and/or cytoplasmic staining), 2+ (medium-intensity complete membrane staining), and 3+ (strong membrane staining).

## Microarray and computational analysis

Microarray analysis of the purified RNA obtained from the exosomes of 7 HBV[+] HCC liver tissue samples and 7 HBV[-] HCC liver tissue samples was performed using human miRNA 8x60K (Agilent Technologies, Santa Clara, CA, USA). Agilent's miRNA Complete Labeling and Hybridization Kit was used to label and hybridize exosomal miRNAs according to the manufacturer's instructions. The microarray slides were scanned with an Agilent Microarray Scanner, and microarray images were analyzed using Agilent Feature Extraction software version 10.7. The differential expression patterns of mRNA and miRNA in HBV[+] and HBV[-] HCC samples were compared using a heat map.

## Exosome coculture with macrophages in vitro

M1-type macrophages and HepG2 cells ($1{\times}10^6$/well) were seeded in a 12-well plate for coculturing. After 24 hours

of incubation, the cells were collected for flow cytometry, Western blotting, and quantitative polymerase chain reaction (qPCR) analysis.

### Western blot analysis

Whole-cell protein extracts were collected using radioimmunoprecipitation assay (RIPA) lysis buffer (Beyotime, Shanghai, China). The Bio-Rad protein assay kit (cat. No. 5000002, Bio-Rad Laboratories, Hercules, CA, USA) was then used to determine the concentration of protein. An equivalent volume of protein was loaded on 10% sodium dodecyl sulphate-polyacrylamide gel electrophoresis (SDS-PAGE) and transferred to 0.22 µm polyvinylidene difluoride (PVDF) membranes (Millipore, St. Louis, MO, USA). The membranes were then incubated with 5% non-fat dry milk (Sigma-Aldrich) for 1 hour, followed by immunoblotting using anti-HSP70 (1:500, ab2787; Abcam, Cambridge, MA, USA), anti-CD63 (1:1,000, ab134045; Abcam), anti-TSG101 (1:1,000, ab125011; Abcam), anti-CD9 (1:1,000, ab236630; Abcam), anti-CD81 (1:700, ab109201; Abcam), anti-COX2 (1:1,000, ab169782 ; Abcam), ACSL4 (1:1,000, ab155282; Abcam), anti-GPX4 (1:1,000, ab125066; Abcam), anti-NOX1 (1:500, ab121009; Abcam), anti-SLC3A2 (1:500, ab253273; Abcam), and anti-GAPDH (1:2,500, ab9485; Abcam) at 4 ℃. The secondary antibody was then incubated for 1 hour at 24 ℃. Finally, the enhanced chemiluminescence (ECL) Western Blotting Detection Kit (Amersham Pharmacia Biotech, Amersham, UK) was used to detect the immunoblots. The quantification of Western blot analysis was measured using Image-Pro Plus 6.0.

### Reactive oxygen species (ROS) measurement by flow cytometry

2',7'-dichlorodihydrofluorescein diacetate (DCFH-DA, 5 µM, Beyotime) was used to detect intracellular ROS levels. In brief, the cells were incubated with DCFH-DA ester at 37 ℃ for 30 minutes. DCF fluorescence of cells was detected by a flow cytometer (FlowJo, version 10.0, BD Biosciences, Franklin Lakes, NJ, USA) at an excitation wavelength of 480 nm and an emission wavelength of 525 nm. Finally, results were analyzed using FlowJo version 10.0.7 software.

### Colony formation assays

The collected cells were digested with trypsin, centrifuged at 1,500 rpm at 25 ℃ for 5 minutes, and resuspended in complete medium. The cells were then seeded into a 6-well plate (500 cells/well) containing 2 mL of complete medium and maintained at 37 ℃ and 5% $CO_2$ for 2 to 3 weeks. The culture medium was removed once the colonies were visible to the naked eye. The cells were rinsed twice in PBS and then fixed with 1.5 mL formaldehyde for 15 minutes. The cells were then stained with 1 mL Giemsa solution in the dark for 20 minutes. The Giemsa solution was then washed away with running water. Finally, the plates were air-dried in an inverted position and the number of cells was counted.

### Invasion and migration assays

Transwell invasion assay was performed using a 24-well Transwell chamber. Invasion was measured using Transwell plates with an 8 µm porous membrane containing Matrigel (BD Biosciences), and migration was measured using Matrigel-free Transwell plates. A density of $4×10^5$ cells were seeded into the upper chamber and 600 µL medium containing 10% FBS was added to the lower chamber. After incubation at 37 ℃ for 24 hours, cells on the upper side of the membrane were removed with clean swabs. Finally, the cells were fixed on the bottom of the membrane with 4% paraformaldehyde for 10 minutes and then stained with 0.4% crystal violet solution. The invading cells were imaged using a Leica DM IL LED inverted microscope (Leica Microsystems GmbH, Wetzlar, Germany).

### TUNEL assay

A TUNEL assay was performed to measure apoptosis. The cells were fixed with 4% paraformaldehyde for 15 minutes and permeabilized in 0.25% Triton-X 100 for 10 minutes. The cells were then covered with 100 µL of equilibration buffer at room temperature for 10 minutes. Finally, the cells were incubated with 50 µL of terminal deoxynucleotidyl transferase (TdT) reaction mixture at 37 ℃ for 45 minutes and then treated with Click-iT reaction mixture. The nuclei were stained with hematoxylin or methyl green. The images were obtained by fluorescence microscope.

### Luciferase reporter assay

SLC3A2 was predicted to be a target of miR-142-3p by TargetScan. The luciferase reporter vector containing wild-type (WT) or mutant (MUT) 3'-UTR of SLC3A2 and

**Table 1** Primer sequences for RT-qPCR

| Gene name | Forward (5' to 3') | Reverse (5' to 3') |
|---|---|---|
| miR-142-3p | GTCGTATCCAGTGCAGGG | CGACGTGTAGTGTTTCCTA |
| miR-375 | GTGCAGGGTCCGAGGT | AGCCGTTTGTTCGTTCGGCT |
| miR-370 | GCCTGCTGGGGTGGAACCTGGTAA | GCGAGCACAGAATTAATACGAC |
| miR-378a | GGTGGTGCCGCAAGAGAATC | TGCAGGAACAACCAGAAAACAT |
| miR-29b-3p | UAGCACCAUUUGAAAUC | GTGCAGGGTCCGAGGT |
| miR-21 | TAGCTTATCAGACTGAGTTG | GCTGTCAACGATACGCTACGTAACG |
| miR-195a-5p | GCGTAGCAGCACAGAAATATTGGC | CTGTCGTCGTAGAGCCAGGGAA |
| COX-2 | CTGCGCCTTTTCAAGGATGG | GGGGATACACCTCTCCACCA |
| ACSL4 | CTCACATTATATTGCTGCCTGT | GGCTGAGAATTCGTGCATGG |
| GPX4 | CCTCCCCAGTACTGCAACAG | GGCTGAGAATTCGTGCATGG |
| PTGS2 | TGTGACTGTA CCCGGACTGG | TGCACATTGTAAGTAGGTGGAC |
| NOX1 | CCTGATTCCTGTGTGTCGAAA | TTGG CTTCTTCTTGTAGCGTTC |
| U6 | CTCGCTTCGGCAGCACA | AACGCTTCACGAATTTGCGT |
| GAPDH | TATCGTGATGCTAGTCCGATG | TGCAGCTAGCTGCATCGATCGG |

miR-142-3p mimic/inhibitor were cotransfected into 293T cells. After cell transfection for 24 to 48 hours, luciferase activity was measured using a Dual-Luciferase Reporter Assay System (Promega, Madison, WI, USA).

### Quantitative reverse transcription polymerase chain reaction (RT-qPCR)

Total RNA was extracted using Trizol reagent (Invitrogen). RNA concentration and quality were tested using the NanoDrop 1000 spectrophotometer (NanoDrop Technologies, Wilmington, DE, USA) and agarose gel electrophoresis (Invitrogen). RT-qPCR analysis was performed using SYBR Premix Ex Taq mix (Takara Bio Inc., Kusatsu, Shiga, Japan) on a real-time PCR system (Thermo Fisher Scientific) following the manufacturer's instructions. Levels of miRNA and mRNA were normalized to U6 and GAPDH, respectively. Finally, the $2^{-\Delta\Delta Ct}$ method was used to calculate the relative expression levels of genes. The primer sequences used in the study are shown in *Table 1*.

### Malondialdehyde (MDA) assay

Serum MDA content in the cells was measured using a thiobarbituric acid reactive substance (TBARS) assay kit (item number: 10009055, Cayman Chemical, Ann Arbor, MI, USA) to monitor lipid peroxidation. Each sample was placed in a 96-well plate, and absorbance was measured at 535 nm with a microplate reader (BioTek, Winooski, VT, USA).

### Determination of glutathione (GSH) levels

GSH levels were measured using a GSH assay kit (Beyotime) according to the manufacturer's protocols. Cells ($1 \times 10^5$) were mixed with 500 µL of 10% metaphosphoric acid and then frozen and thawed twice using liquid nitrogen and 37 ℃ water. The sample was centrifuged at 10,000 rpm at 4 ℃ for 10 minutes. The supernatant was then collected and seeded into a 96-well plate with 150-µL total GSH assay reagent added to each well. The absorbance was measured at 412 nm with a microplate reader (BioTek).

### Measurement of Fe²⁺

The $Fe^{2+}$ assays were performed according to the manufacturer's instructions. The level of $Fe^{2+}$ in cells was measured using a microplate reader (BioTek) at an absorption wavelength of 593 nm.

### Statistical analysis

All experiment values are expressed as mean ± standard

    

deviation (SD). All experiments were carried out 3 times. GraphPad Prism 8 software was used, and the data were analyzed using the Student's *t*-test and one-way analysis of variance (ANOVA). P<0.05 was considered statistically significant.

## Results

### The impact of HBV⁺ infection on HCC

HCC tissues were obtained from clinical HCC tissue specimens, and IHC staining was used to detect expression levels of M1 and M2 macrophages. The results showed that the level of CD80⁺ M1-type macrophages in clinical samples of HBV⁺ HCC tissue [HBV⁺ live cancer (LC) tissue] was significantly lower than the level in clinical samples of HBV⁻ HCC tissue (HBV⁻ LC tissue). However, there was no significant difference between the 2 samples in CD163⁺ M2-type macrophages (*Figure 1A*). In order to characterize exosomes, Western blot analysis was used to confirm that particles expressed HSP70, CD63, TSG101, and CD81, and that these were highly expressed in particles isolated from HBV⁺ tissue (P<0.001) (*Figure 1B*). The results showed that compared with the NC group, SLC3A2 expression was significantly lower in the HBV⁺ group and HBV⁻ group, and the expression level was the lowest in the HBV⁺ group (P<0.001) (*Figure 1C*). In summary, the expression level of M1 macrophages and SLC3A2 in HBV⁺ HCC tissues was low, and exosomes were successfully isolated from the HBV⁺ HCC group.

### Differential expression of miRNAs in exosomes of HBV-HCC cells

The differential expression of miRNAs in exosomes of HCC cells was detected by RT-qPCR. The results showed that compared with normal HCC cells, miR-142-3p, miR-375, miR-370, miR-29b-3p, and miR-21 were significantly upregulated in the HBV⁺ and HBV⁻ groups, while miR-378a and miR-195a-5p was significantly downregulated in the HBV⁺ and HBV⁻ groups. In addition, miR-142-3p was most significantly differentially expressed in the HBV⁺ group (*Figure 2*).

### The effect of miR-142-3p on the lipid metabolism of ferroptosis in cells

To explore the effect of miR-142-3p on the ferroptosis

lipid metabolism of M1 macrophages, we detected the expression levels of GSH, MDA, and Fe²⁺ in macrophages (*Figure 3A-3C*). The results showed that miR-142-3p inhibitor significantly inhibited the expression level of MDA and Fe²⁺ in cells and cell proliferation (P<0.01), while the expression level of MDA increased significantly (P<0.01). In addition, we found that miR-142-3p inhibitors significantly increased the colony formation rate of macrophages (P<0.05) (*Figure 3D,3E*). In summary, miR-142-3p affected the ferroptosis lipid metabolism of M1 macrophages.

### MiR-142-3p target regulates SLC3A2

In order to explain the mechanism of miR-142-3p in HBV-induced ferroptosis of HCC cells, we used the bioinformatics website "Starbase" to identify the mRNA regulated by miR-142-3p, which was SLC3A2 (*Figure 4A*). To investigate whether miR-142-3p directly targeted the SLC3A2 3'-UTR, a luciferase reporter vector was constructed carrying the SLC3A2 3'-UTR containing the specific seed sequence of miR-142-3p mimic into the Huh-7 cell line. As determined by luciferase activity assay, miR-142-3p noticeably suppressed relative luciferase activity in the presence of the WT reporter construct of SLC3A2 3'-UTR (P<0.0.5), while there was no significant difference in the presence of the MUT reporter construct of SLC3A2 3'-UTR (*Figure 4B*), suggesting that miR-142-3p directly targeted SLC3A2. The expression level of SLC3A2 was evaluated after transfection with miR-142-3p mimic and was found to have decreased (*Figure 4C*). Therefore, we speculated that miR-142-3p participated in the regulation of HBV-induced ferroptosis of HCC cells through SLC3A2.

### MiR-142-3p regulates the ferroptosis of M1 macrophages under HBV infection by targeting SLC3A2

We confirmed the role of SLC3A2 in miR-142-3p regulation of ferroptosis in HBV-infected HCC cells. The results of Western blotting and RT-qPCR showed that compared with the NC group, HBV⁺ significantly increased protein and mRNA expression of COX2, ACSL4, NOX1, PTGS2, and GPX4 (P<0.01), and cotransfection with miR-142-3p inhibitor or pcDNA3.1-SLC3A2 increased the expression level of these proteins and mRNA (P<0.01). In addition, compared with the miR-142-3p inhibitor group, protein and mRNA expression levels of COX2, ACSL4,
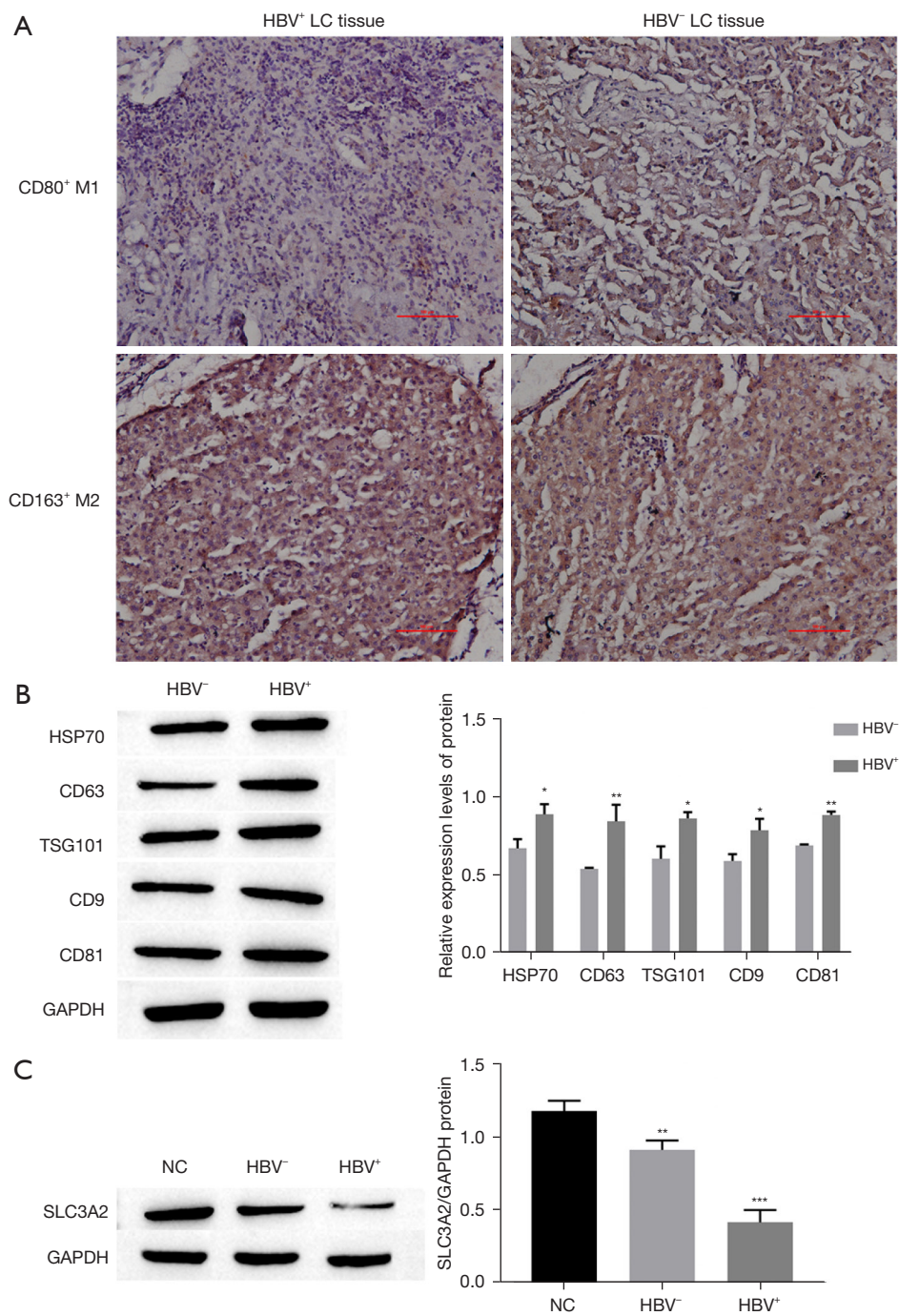
**Figure 1** The impact of HBV[+] infection on HCC. (A) The expression of M1-type macrophages and M2-type macrophages in HCC tissues was stained by immunohistochemistry (scale bar: 100 μm). (B) The molecular markers of exosomes were detected by Western blot. (C) The expression of SLC3A2 was detected by Western blot. Data are mean ± SD. Compared with the NC group: *, P<0.05; **, P<0.01; ***, P<0.001. HBV, hepatitis B virus; HCC, hepatocellular carcinoma; LC, live cancer; NC, negative control; SD, standard deviation.
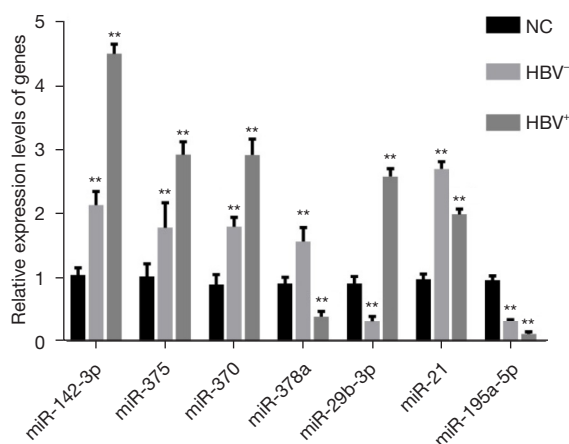
**Figure 2** HBV+ HCC exosomal miRNA was detected by RT-qPCR. Data are mean ± SD. Compared with the NC group: **, P<0.01. HBV, hepatitis B virus; HCC, hepatocellular carcinoma; NC, negative control; RT-qPCR, quantitative reverse transcription polymerase chain reaction; SD, standard deviation.

NOX1, PTGS2, and GPX4 were significantly increased when cocultured with miR-142-3p inhibitor and si-SLC3A2 (*Figure 5A,5B*) (P<0.01). To further confirm the role of SLC3A2 in miR-142-3p in regulating ferroptosis of HBV-infected HCC cells, we investigated the expression levels of GSH, MDA, and $Fe^{2+}$ by enzyme-linked immunosorbent *assay* (ELISA) (*Figure 5C-5E*). The results showed that compared with the NC group, MDA and $Fe^{2+}$ content in cells was significantly increased after HBV induction (P<0.01), while GSH content was significantly reduced (P<0.01). This effect was significantly reversed by miR-142-3p inhibitor or pcDNA3.1-SLC3A2 treatment (P<0.01). It is worth noting that compared with the HBV+ + miR-142-3p inhibitor group, when cocultured with miR-142-3p inhibitor and si-SLC3A2 at the same time, the content of MDA, $Fe^{2+}$, and GSH was significantly reduced. ROS accumulation is regarded as a hallmark of ferroptosis. To determine whether ROS played a key role in HBV-induced cell death, we measured intracellular ROS levels by using the oxidation-sensitive fluorescent probe DCFH-DA. The results showed that HBV+ increased the level of intracellular ROS (*Figure 5F*). In addition, this effect was reversed by miR-142-3p inhibitor or pcDNA3.1-SLC3A2. The results of the TUNEL assay to determine cell ferroptosis were consistent with the previous results. HBV+ induced cell ferroptosis to increase, and miR-142-3p inhibitor or pcDNA3.1-SLC3A2 reduced cell ferroptosis (*Figure 5G*). Taken together, these data indicated that miR-142-3p

increased cell ferroptosis by inhibiting SLC3A2.

### *MiR-142-3p promotes the proliferation, migration, and invasion of HCC cells by inhibiting SLC3A2*

This study also confirmed the effect of miR-142-3p via SLC3A2 on the malignant behavior of HCC cells, including migration, invasion, and colony formation. HBV+ induction significantly increased the proliferation, invasion, and proliferation of HCC cells compared with the NC group (*Figure 6*). In addition, miR-142-3p inhibitor, pcDNA3.1-SLC3A2, miR-142-3p inhibitor + si-SLC3A2, and pcDNA3.1-SLC3A2 + Zileuton treatment reversed these effects, suggesting that miR-142-3p inhibited the proliferation, invasion, and proliferation of HCC cells through SLC3A2.

### Discussion

Exosomes are endogenous nanovesicles with a double-layer membrane which regulate various physiological and pathological processes by transmitting biological signals between cells (19). The role of exosomes in mediating the spread of HBV between cells has been widely demonstrated (20). However, the role of exosomes in HBV infection has not been elucidated so far. In the present study, we found that M1 macrophages had low expression levels in HBV+-induced HCC tissue, and exosome miR-143-3p had high expression levels. The results indicated that miR-142-3p and M1 macrophages are closely related to the development of HBV+-induced HCC.

There is increasing evidence that long non-coding RNA (lncRNA) plays an important role in tumor progression. MiR-142-3p has been proven to be a tumor suppressor in a variety of malignant tumors (21,22). In osteosarcoma, miR-143-3p was shown to inhibit the proliferation, migration, and invasion of osteosarcoma by targeting HMGA1 (23). A recent study reported that miR-142-3p was downregulated in HCC, and its overexpression inhibited the proliferation of HCC cells (18). The increased expression of miR-142-3p in HBV+-induced HCC is consistent with the results of this paper (24). In addition, through "Starbase", we predicted the potential mRNA of miR-142-3p and found that miR-142-3p and SLC3A2 had binding sites. Studies have shown that SLC3A2 is a major functional subunit of XC− system and inhibition of XC− induces ferroptosis (25). At the same time, Kaplan-Meier survival analysis demonstrated that low SLC3A2 or SLC7A11 expression and high expression of
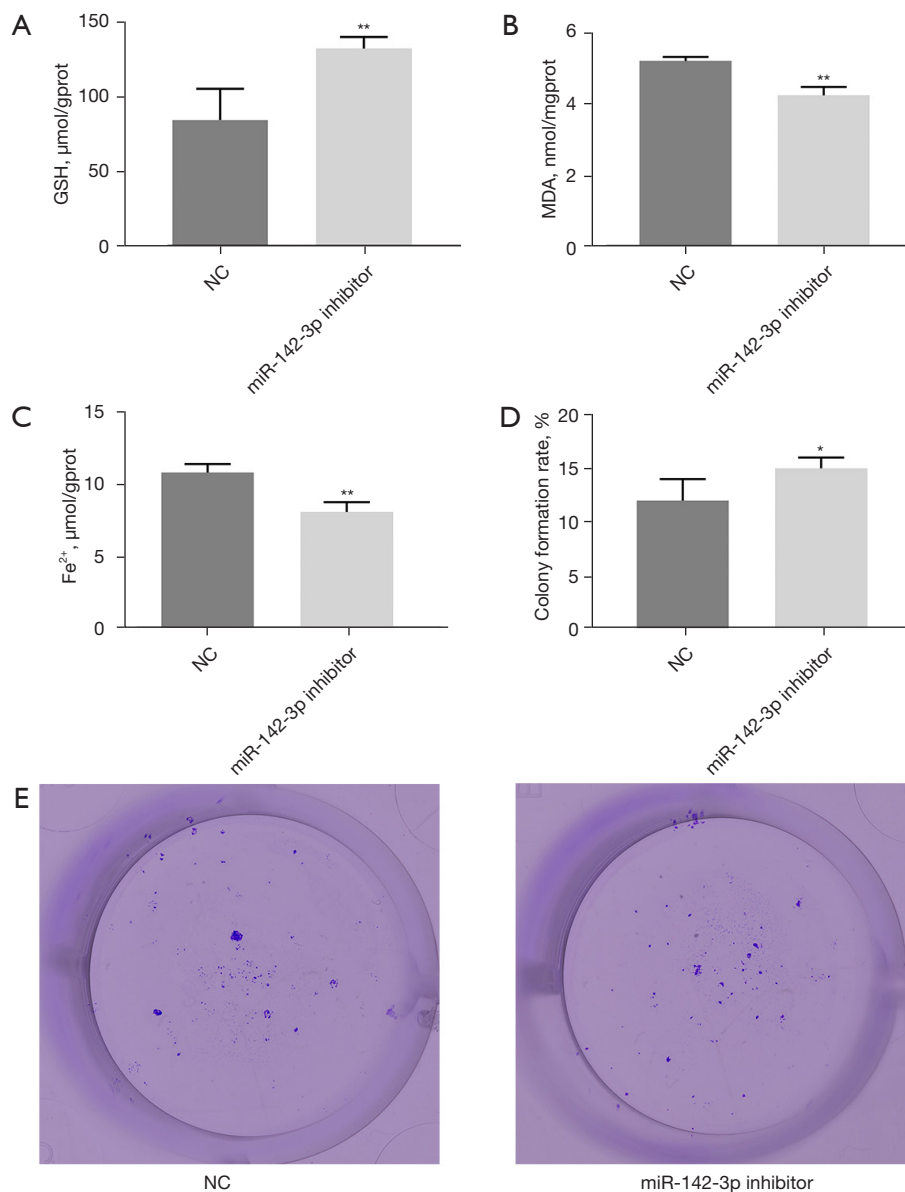
**Figure 3** The effect of miR-142-3p on the lipid metabolism of ferroptosis in HCC cells. (A) The content of GSH was tested using a GSH enzyme-linked immunoassay kit. (B) The content of MDA was tested using an MDA enzyme-linked immunoassay kit. (C) The content of $Fe^{2+}$ was tested using an $Fe^{2+}$ enzyme-linked immunoassay kit. (D) The rate of cell colony formation was determined. (E) Cell proliferation was measured by a colony formation experiment (Giemsa stain). Aperture =16 mm. Data are mean ± SD. NC group: HBV+ induced M1 macrophages; miR-142-3p inhibitor: HBV+ + inhibitor. Compared with the NC group: *, $P<0.05$; **, $P<0.01$. GSH, glutathione; HCC, hepatocellular carcinoma; MDA, malondialdehyde; NC, negative control; SD, standard deviation.

CD8A were associated with good overall survival (OS) or disease-free survival (DFS) in HCC patients (26).

Ferroptosis is a newly discovered form of cell death, which is different from autophagy, apoptosis, pyrolysis, or necrosis. The main feature of ferroptosis is the accumulation of lipid peroxidation products in a cellular iron-dependent manner (27). However, there is no specific indicator for the detection of ferroptosis (28). Generally, ferroptosis is caused by a combination of changes in GPX4, $Fe^{2+}$, GSH, and ROS levels. Accumulating research has demonstrated
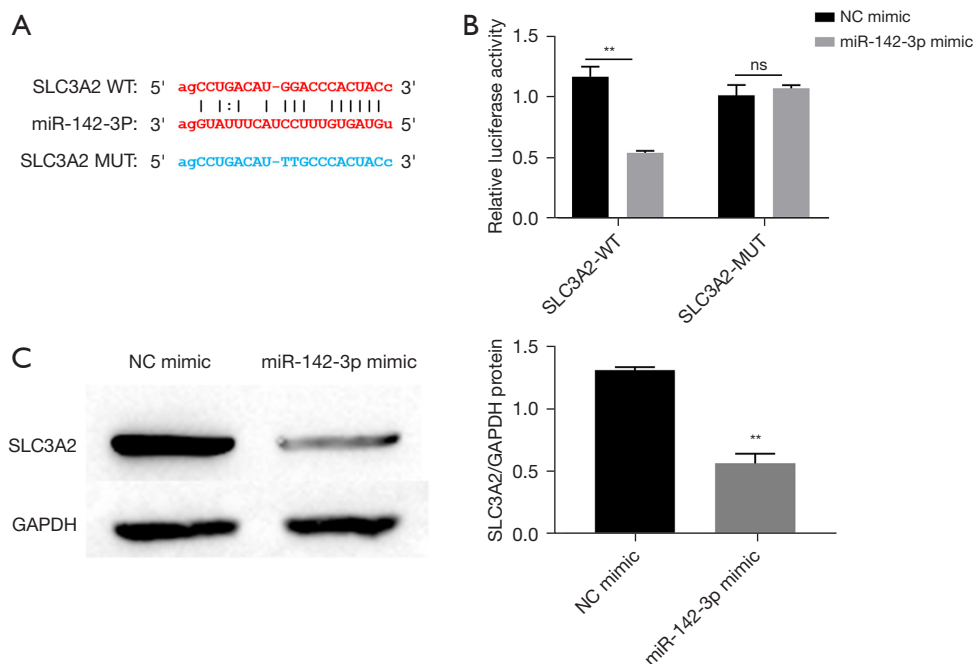
**Figure 4** Targeting relationship of miR-142-3p and SLC3A2. (A) MiR-142-3p binding sites in the 3'-UTR of SLC3A2 were predicted by TargetScan. The sequences of the MUT and WT SLC3A2 3'-UTR were used for the dual luciferase reporter construct. (B) Dual luciferase reporter gene assay was used to detect the targeting of miR-142-3p and SLC3A2. (C) The expression of SLC3A2 was determined by Western blot. Data are mean ± SD. **, P<0.01. MUT, mutant; NC, negative control; ns, not significant; UTR, untranslated region; WT, wild type.
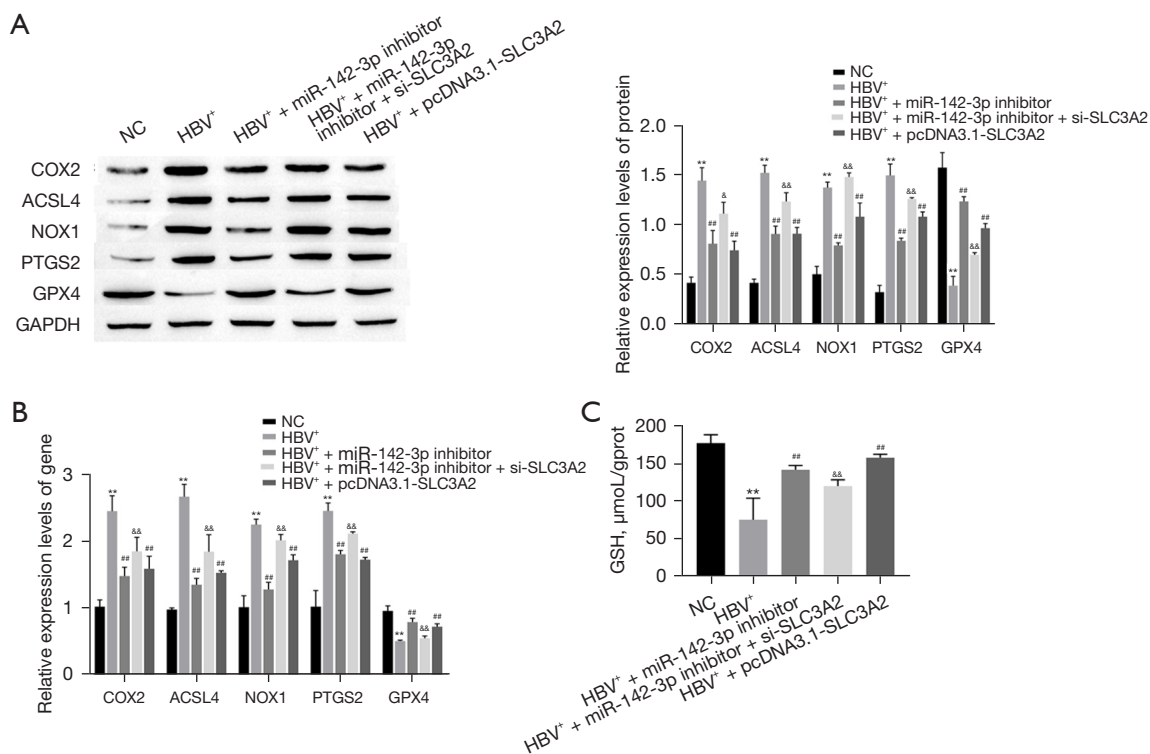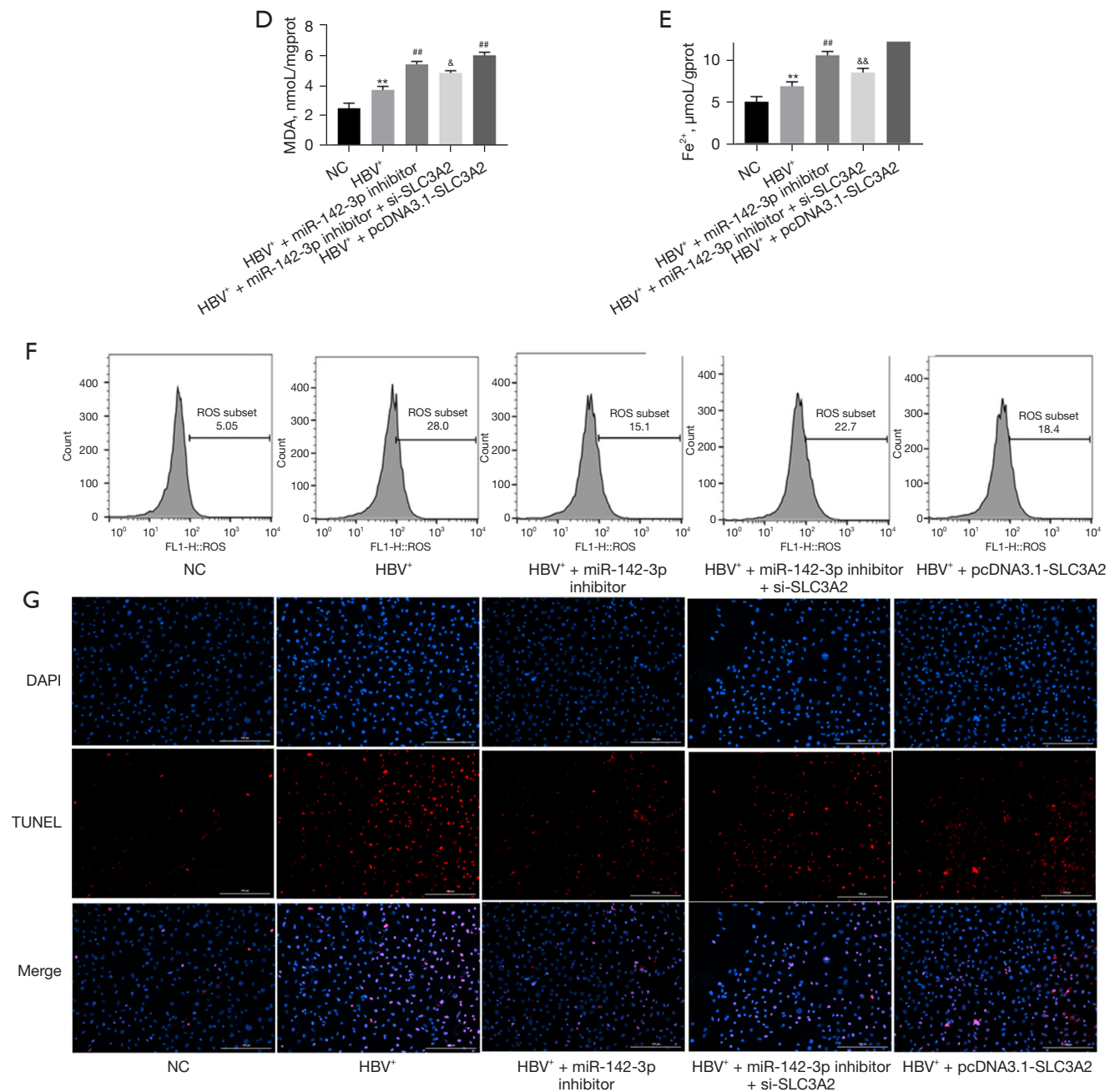
**Figure 5** MiR-142-3p regulates HCC cell ferroptosis under HBV infection by targeting SLC3A2. (A) The protein expression of COX2, ACSL4, NOX1, PTGS2, and GPX4 was determined by Western blot. (B) The gene expression of COX2, ACSL4, NOX1, PTGS2, and GPX4 was determined by RT-qPCR. (C) The content of GSH was tested using a GSH enzyme-linked immunoassay kit. (D) The content of MDA was tested using an MDA enzyme-linked immunoassay kit. (E) The content of $Fe^{2+}$ was tested using an $Fe^{2+}$ enzyme-linked immunoassay kit. (F) Flow cytometry was used to analyze ROS. (G) TUNEL detected cellular ferroptosis (scale bar: 200 μm). Data are mean ± SD. Compared with the NC group: **, P<0.01. Compared with the HBV+ group: ##, P<0.01. Compared with the HBV+ + miR-142-3p inhibitor group: &, P<0.05; &&, P<0.01. GSH, glutathione; HBV, hepatitis B virus; HCC, hepatocellular carcinoma; MDA, malondialdehyde; NC, negative control; ROS, reactive oxygen species; SD, standard deviation.
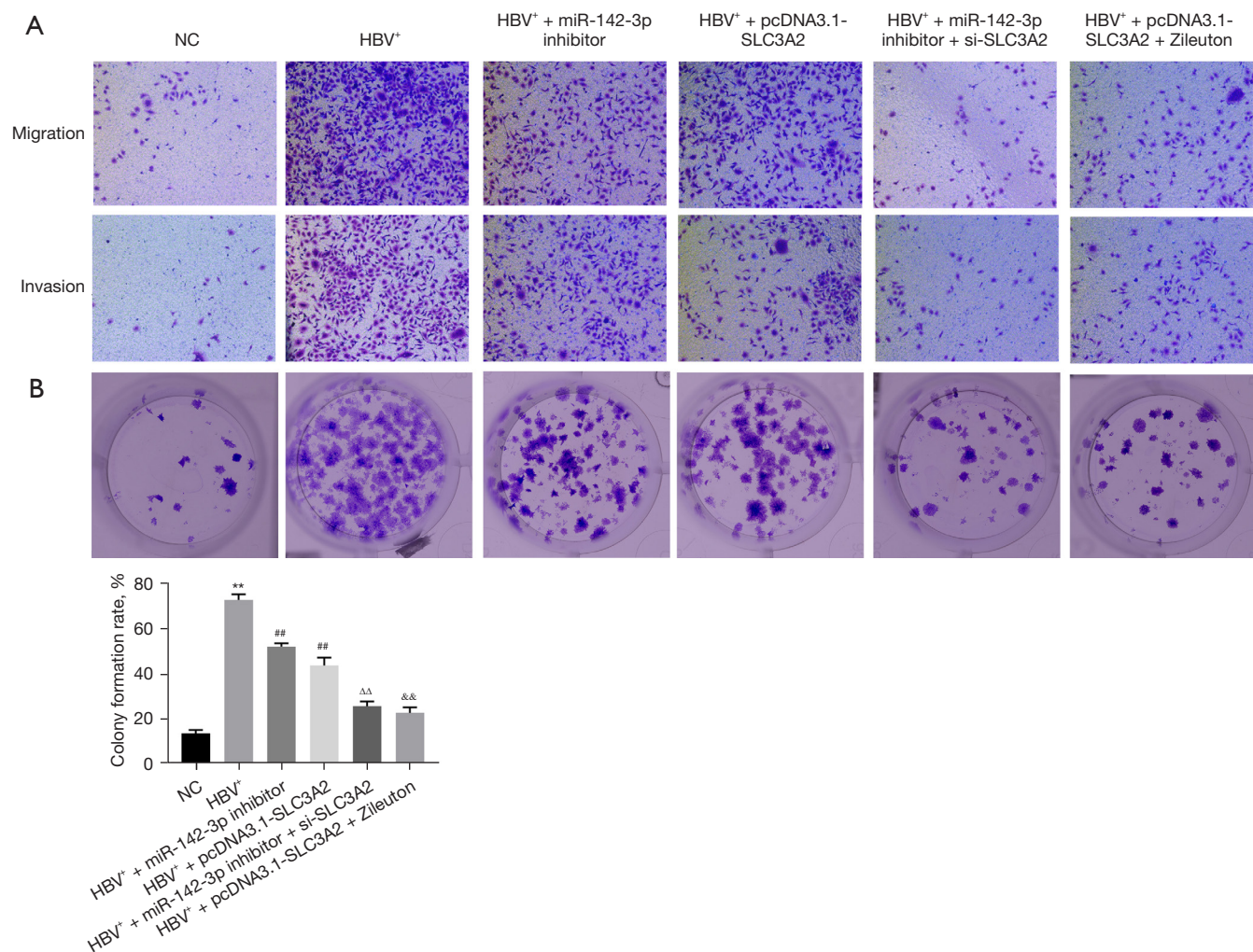
**Figure 6** The effect of miR-142-3p on the proliferation, migration, and invasion of HCC cells through SLC3A2. (A) Cell migration and invasion were detected by Transwell assay (crystal violet stain; magnification: 200×). (B) Cell proliferation was measured by a colony formation experiment. Data are mean ± SD. Compared with the NC group: **, P<0.01. Compared with the HBV⁺ group: ##, P<0.01. Compared with the HBV⁺ + miR-142-3p inhibitor group: &&, P<0.01. Compared with the HBV⁺ + pcDNA3.1-SLC3A2 group: ΔΔ, P<0.01. HBV, hepatitis B virus; HCC, hepatocellular carcinoma; NC, negative control; SD, standard deviation.

that ferroptosis is related to a variety of cancers (29,30). Recent studies have shown that activation of ferroptosis-related pathways can effectively prevent tumor progression and enhance the effects of chemotherapy, targeted therapy, and even immunotherapy (31,32). Previous evidence has shown that inhibiting ferroptosis can achieve ideal therapeutic effects in neurodegenerative diseases, including stroke (33). In this study, we measured levels of GSH, $Fe^{2+}$, GPX4, ROS, and ferroptosis marker proteins COX2, ACSL4, NOX1, PTGS2, and GPX4. In addition, cell death was measured by TUNEL assay. We found that HBV⁺ induced the ferroptosis of M1 macrophages, and miR-142-3p promoted the ferroptosis of M1 macrophages through SLC3A2.

In summary, our study showed that miR-142-3p promoted HBV-induced ferroptosis of M1 macrophages by regulating SLC3A2, accelerating the development of HCC. The regulation of miR-142-3p and its target SLC3A2 will help to clarify the pathogenesis of HCC induced by HBV infection and provide new theoretical foundations and

therapeutic targets.

## Footnote

*Reporting Checklist:* The authors have completed the MDAR reporting checklist. Available at https://jgo.amegroups.com/article/view/10.21037/jgo-21-916/rc

*Data Sharing Statement:* Available at https://jgo.amegroups.com/article/view/10.21037/jgo-21-916/dss

*Conflicts of Interest:* All authors have completed the ICMJE uniform disclosure form (available at https://jgo.amegroups.com/article/view/10.21037/jgo-21-916/coif). The authors have no conflicts of interest to declare.

*Ethical Statement:* The authors are accountable for all aspects of the work in ensuring that questions related to the accuracy or integrity of any part of the work are appropriately investigated and resolved. The study was conducted in accordance with the Declaration of Helsinki (as revised in 2013). The study was approved by Medical Ethics Committee of the First People's Hospital of Kunming (No. YLS2020-08) and informed consent was taken from all the patients.

## References

1. Song X, Tan S, Wu Z, et al. HBV suppresses ZHX2 expression to promote proliferation of HCC through miR-155 activation. Int J Cancer 2018;143:3120-30.
2. Beasley RP, Hwang LY, Lin CC, et al. Hepatocellular carcinoma and hepatitis B virus. A prospective study of 22 707 men in Taiwan. Lancet 1981;2:1129-33.
3. Shlomai A, de Jong YP, Rice CM. Virus associated malignancies: the role of viral hepatitis in hepatocellular carcinoma. Semin Cancer Biol 2014;26:78-88.
4. Bertoletti A, Ferrari C. Innate and adaptive immune responses in chronic hepatitis B virus infections: towards restoration of immune control of viral infection. Postgrad Med J 2013;89:294-304.
5. Gordon S, Martinez FO. Alternative activation of macrophages: mechanism and functions. Immunity 2010;32:593-604.
6. Affo S, Yu LX, Schwabe RF. The Role of Cancer-Associated Fibroblasts and Fibrosis in Liver Cancer. Annu Rev Pathol 2017;12:153-86.
7. Xie L, Yang Y, Meng J, et al. Cationic polysaccharide spermine-pullulan drives tumor associated macrophage towards M1 phenotype to inhibit tumor progression. Int J Biol Macromol 2019;123:1012-9.
8. Ding T, Xu J, Wang F, et al. High tumor-infiltrating macrophage density predicts poor prognosis in patients with primary hepatocellular carcinoma after resection. Hum Pathol 2009;40:381-9.
9. Schorey JS, Cheng Y, Singh PP, et al. Exosomes and other extracellular vesicles in host-pathogen interactions. EMBO Rep 2015;16:24-43.
10. Chen Q, Li Y, Liu Y, et al. Exosomal Non-coding RNAs-Mediated Crosstalk in the Tumor Microenvironment. Front Cell Dev Biol 2021;9:646864.
11. Bartel DP. MicroRNAs: target recognition and regulatory functions. Cell 2009;136:215-33.
12. Bandopadhyay M, Bharadwaj M. Exosomal miRNAs in hepatitis B virus related liver disease: a new hope for biomarker. Gut Pathog 2020;12:23.
13. Dai X, Zhang W, Zhang H, et al. Modulation of HBV replication by microRNA-15b through targeting hepatocyte nuclear factor 1α. Nucleic Acids Res 2014;42:6578-90.

14. Jin J, Tang S, Xia L, et al. MicroRNA-501 promotes HBV replication by targeting HBXIP. Biochem Biophys Res Commun 2013;430:1228-33.

15. Kim JH, Lee CH, Lee SW. Exosomal Transmission of MicroRNA from HCV Replicating Cells Stimulates Transdifferentiation in Hepatic Stellate Cells. Mol Ther Nucleic Acids 2019;14:483-97.

16. Sonda N, Simonato F, Peranzoni E, et al. miR-142-3p prevents macrophage differentiation during cancer-induced myelopoiesis. Immunity 2013;38:1236-49.

17. Zhang Q, Qu Y, Zhang Q, et al. Exosomes derived from hepatitis B virus-infected hepatocytes promote liver fibrosis via miR-222/TFRC axis. Cell Biol Toxicol 2022. [Epub ahead of print].

18. Fu Y, Sun LQ, Huang Y, et al. miR-142-3p Inhibits the Metastasis of Hepatocellular Carcinoma Cells by Regulating HMGB1 Gene Expression. Curr Mol Med 2018;18:135-41.

19. Li S, Li S, Wu S, et al. Exosomes Modulate the Viral Replication and Host Immune Responses in HBV Infection. Biomed Res Int 2019;2019:2103943.

20. Shen J, Huang CK, Yu H, et al. The role of exosomes in hepatitis, liver cirrhosis and hepatocellular carcinoma. J Cell Mol Med 2017;21:986-92.

21. Troschel FM, Böhly N, Borrmann K, et al. miR-142-3p attenuates breast cancer stem cell characteristics and decreases radioresistance in vitro. Tumour Biol 2018;40:1010428318791887.

22. Tan YF, Chen ZY, Wang L, et al. MiR-142-3p functions as an oncogene in prostate cancer by targeting FOXO1. J Cancer 2020;11:1614-24.

23. Xu G, Wang J, Jia Y, et al. MiR-142-3p functions as a potential tumor suppressor in human osteosarcoma by targeting HMGA1. Cell Physiol Biochem 2014;33:1329-39.

24. Ghosh A, Ghosh A, Datta S, et al. Hepatic miR-126 is a potential plasma biomarker for detection of hepatitis B virus infected hepatocellular carcinoma. Int J Cancer 2016;138:2732-44.

25. Ma L, Zhang X, Yu K, et al. Targeting SLC3A2 subunit of system XC- is essential for m6A reader YTHDC2 to be an endogenous ferroptosis inducer in lung adenocarcinoma. Free Radic Biol Med 2021;168:25-43.

26. Kong R, Wang N, Han W, et al. IFNγ-mediated repression of system xc- drives vulnerability to induced ferroptosis in hepatocellular carcinoma cells. J Leukoc Biol 2021;110:301-14.

27. Dixon SJ, Lemberg KM, Lamprecht MR, et al. Ferroptosis: an iron-dependent form of nonapoptotic cell death. Cell 2012;149:1060-72.

28. Chen D, Eyupoglu IY, Savaskan N. Ferroptosis and Cell Death Analysis by Flow Cytometry. Methods Mol Biol 2017;1601:71-7.

29. Zhi T, Jiang K, Zhang C, et al. MicroRNA-1301 inhibits proliferation of human glioma cells by directly targeting N-Ras. Am J Cancer Res 2017;7:982-98.

30. Kenny EM, Fidan E, Yang Q, et al. Ferroptosis Contributes to Neuronal Death and Functional Outcome After Traumatic Brain Injury. Crit Care Med 2019;47:410-8.

31. Wang W, Green M, Choi JE, et al. CD8+ T cells regulate tumour ferroptosis during cancer immunotherapy. Nature 2019;569:270-4.

32. Sun X, Niu X, Chen R, et al. Metallothionein-1G facilitates sorafenib resistance through inhibition of ferroptosis. Hepatology 2016;64:488-500.

33. Tang M, Chen Z, Wu D, et al. Ferritinophagy/ferroptosis: Iron-related newcomers in human diseases. J Cell Physiol 2018;233:9179-90.

(English Language Editor: A. Muijlwijk)